

# C5aR1 blockade reshapes immunosuppressive tumor microenvironment and synergizes with immune checkpoint blockade therapy in high-grade serous ovarian cancer

Chen Zhang<sup>a\*</sup>, Kankan Cao<sup>a\*</sup>, Moran Yang<sup>a</sup>, Yiyang Wang<sup>a</sup>, Mengdi He<sup>a</sup>, Jiaqi Lu<sup>b</sup>, Yan Huang<sup>c</sup>, Guodong Zhang<sup>a,b</sup>, and Haiou Liu<sup>id</sup><sup>a</sup>

<sup>a</sup>Shanghai Key Laboratory of Female Reproductive Endocrine Related Diseases, Obstetrics and Gynecology Hospital, Fudan University, Shanghai, China; <sup>b</sup>Department of Gynecology, Obstetrics and Gynecology Hospital, Fudan University, Shanghai, China; <sup>c</sup>Department of Gynecologic Oncology, Shanghai Cancer Center, Fudan University, Shanghai, China

## ABSTRACT

High-grade serous ovarian cancer (HGSC), with a modest response to immune checkpoint blockade (ICB) targeting PD-1/PD-L1 monotherapy, is densely infiltrated by M2-polarized tumor-associated macrophages (TAMs) and regulatory T (Treg) cells. The complement C5a/C5aR1 axis contributes to the programming of the immunosuppressive phenotype of TAMs in solid tumors and represents a promising immunomodulatory target for treating HGSCs. Here, we aimed to identify the relevance of C5aR1 in prognosis, immune microenvironment, and immunotherapy response in HGSCs. The expression and relationship of C5aR1 with tumor-infiltrating immune cells were assessed by immunohistochemistry and flow cytometry in the training cohort ( $n = 120$ ) and fresh HGSC tissues ( $n = 36$ ). Transcriptomic analyses of the xenografts delineated the mechanisms driving the immunomodulatory activity of PMX53, an orally bioavailable C5aR1 inhibitor. Therapeutic relevance was confirmed in ex vivo tumor cultures and The Cancer Genome Atlas (TCGA) datasets. C5aR1 expression independently predicted dismal prognosis and was linked to the immunoevasive subtype of HGSC, characterized by increased infiltration of pro-tumor cells (Treg cells, M2-polarized macrophages, and neutrophils) and impaired CD8<sup>+</sup>T functions. PMX53 antagonized subcutaneous tumor growth, modulated immunosuppressive mechanisms and synergized with aPD-1 in several tumor types. Single-cell RNA-seq analysis revealed predominant C5aR1 expression in TAMs, with an immunosuppressive-related expression signature in C5aR1<sup>+</sup>TAMs. Furthermore, the combination of C5aR1 and PD-L1 was associated with specific molecular characteristics and matched clinical response annotations. Therefore, the abundance of C5aR1 could predict an inferior prognosis in HGSCs, and incorporating PD-L1 may serve as a novel predictive biomarker to guide therapeutic options.

## ARTICLE HISTORY

Received 24 May 2023  
Revised 5 September 2023  
Accepted 15 September 2023

## KEYWORDS

High-grade serous ovarian cancer; immunotherapy; prognosis; tumor microenvironment; tumor-associated macrophages


## Introduction

Immunotherapy has revolutionized cancer treatment; however, its efficacy remains limited in the clinical setting of ovarian cancer. Results from the phase Ib JAVELIN study and phase II KEYNOTE-100 study indicated that the objective response rate of immune monotherapy in the treatment of ovarian cancer is only approximately 10%, far lower than that of melanoma and lymphoma.<sup>1,2</sup> The dismal efficacy may be due to tumor heterogeneity, presence of immunosuppressive signals that prevent T cell reactivation, and accumulation of immunosuppressive myeloid cells.<sup>3</sup> Accordingly, combination therapies that reverse immunosuppressive pressure against effector cells are under intense investigation.<sup>4</sup> In addition, there is a need to identify molecular markers that can predict the efficacy of immunotherapy in ovarian cancer to screen appropriate immunotherapeutic populations.

Complement C5a exerts immunomodulatory functions through the activation of C5a receptor 1 (C5aR1) in myeloid cells, such as macrophages, monocytes, DCs, and neutrophils.<sup>5</sup> C5a-C5aR1 signaling frequently reshapes the immunosuppressive tumor microenvironment and increases the potential for cancer progression via molecular and cellular events.<sup>6</sup> Recent studies have identified the contribution of C5a-C5aR1 signaling to tumor-associated immune responses through the induction of bioactive molecules, including IL-1 $\beta$ , IL-6, and TNF- $\alpha$ .<sup>7,8</sup> Furthermore, crosstalk between C5aR1 and toll-like receptors (TLR) enhances the production of TNF- $\alpha$  and IFN- $\gamma$  from natural killer and natural killer T cells.<sup>9</sup> C5aR1 blockade also impairs tumor growth and diminishes the recruitment of myeloid-derived suppressor cells (MDSC) into tumors in lung cancer-bearing mice.<sup>8</sup> Although the effect of C5aR1 on the anti-tumor immune response has been reported in several human solid cancers, few studies have addressed its implications in ovarian cancer.

**CONTACT** Haiou Liu  [liuhaiou@fudan.edu.cn](mailto:liuhaiou@fudan.edu.cn); Guodong Zhang  [gdzhang12@fudan.edu.cn](mailto:gdzhang12@fudan.edu.cn)  Shanghai Key Laboratory of Female Reproductive Endocrine Related Diseases, Obstetrics and Gynecology Hospital, Fudan University, No. 128, Shenyang road, Yangpu district, Shanghai 200011, P. R. China; Yan Huang  [huangyan19790315@163.com](mailto:huangyan19790315@163.com)  Department of Gynecologic Oncology, Shanghai Cancer Center, Fudan University, No. 270, Dongan road, Xuhui district, Shanghai 200032, china

\*These authors contributed equally to this work.

 Supplemental data for this article can be accessed online at <https://doi.org/10.1080/2162402X.2023.2261242>

© 2023 The Author(s). Published with license by Taylor & Francis Group, LLC.

This is an Open Access article distributed under the terms of the Creative Commons Attribution-NonCommercial License (<http://creativecommons.org/licenses/by-nc/4.0/>), which permits unrestricted non-commercial use, distribution, and reproduction in any medium, provided the original work is properly cited. The terms on which this article has been published allow the posting of the Accepted Manuscript in a repository by the author(s) or with their consent.

Activation of C5a-C5aR1 signaling has also been shown to have prognostic effects. Overexpression of C5aR1 in non-small cell lung cancer predicts poor prognosis.<sup>10</sup> In breast cancer, C5aR1 expression is associated with larger tumor size, higher proliferation rate, presence of lymph node metastasis, and advanced clinical stages.<sup>11</sup> Correspondingly, patients with C5aR1-positive breast cancer had lower survival rates than those with C5aR1-negative breast cancer. C5aR1 expression has also been associated with prognosis in patients with gastric cancer,<sup>12</sup> hepatocellular carcinoma,<sup>13</sup> urothelial and renal cell carcinoma,<sup>14,15</sup> with lower overall survival rates in patients with high tumor C5aR1 expression. However, the prognostic value of C5aR1 in ovarian cancer has not been fully elucidated.

Here, we established the prognostic value of C5aR1 expression in patients with high-grade serous ovarian cancer (HGSC). In preclinical models, C5aR1 blockade results in a more permissive environment for immune-mediated tumor rejection, and as a result, its combination with anti-PD-1 antibodies synergistically initiates cytotoxic activity. Furthermore, scRNA-seq analysis revealed features and tracked intercellular communication signals in C5aR1<sup>+</sup> macrophages. Finally, we integrated genomic and transcriptomic data to propose potential therapeutic options through the C5aR1 and PD-L1 panel subgroups. Our findings have led to the development of a classification of HGSC based on C5aR1 and PD-L1 expression and its potential to predict responses to immune checkpoint blockade and molecular-targeted therapy.

## Materials and methods

### Ethics approval and consent to participate

The study was approved by the Ethics Committee of the Obstetrics and Gynecology Hospital of Fudan University (Kyy2016–49, Kyy2017–27) and the Ethics Committee of Shanghai Cancer Center (050432-4-2108\*). The study was performed in accordance with the Declaration of Helsinki and all patients provided written informed consent for sample collection and data analyses.

### Patients and specimens

Tissue specimens from 120 patients with HGSC in Discovery cohort who underwent surgery between March 2013 and November 2015 were obtained from the Gynecology and Obstetrics Hospital of Fudan University. None of the patients had severe disease and received chemotherapy, radiation, or any other anti-tumor medicine treatment before surgery. Overall survival (OS) was defined as the period from the date of surgery to the date of death or last follow-up until March 2019. Fresh tumor tissue samples were obtained from 36 patients with HGSC during surgery at the Gynecology and Obstetrics Hospital and Shanghai Cancer Center of Fudan University, including 36 HGSC tissues used for fresh tumor explant cultures. The characteristics of all patients are listed in Supplementary Table S1.

## Immunohistochemistry and evaluation

All specimens were examined using hematoxylin and eosin staining, and two 2.0-mm diameter tissue cores representing the tumor area were selected from each sample to construct tissue microarrays (TMAs). For immunohistochemistry, TMA sections were placed in an oven at 60°C overnight before deparaffinization and rehydration. Antigen retrieval was performed with citrate buffer (pH = 6) for 10 min in a water bath, and endogenous peroxidase blocking was subsequently delivered for 20 min. Sections were incubated with normal goat serum for 30 min to avoid nonspecific staining and then decanted without washing. Sections were incubated with primary antibodies (Supplementary Table S2) at 4°C overnight, and biotin-labeled anti-mouse/rabbit IgG was added for 20 min. After biotin amplification of biotin and horseradish peroxidase signals, the sections were visualized using freshly prepared DAB. The staining results of TMAs were independently assessed by two investigators (M.Y. and Y.W.) who were blinded to the clinicopathological characteristics. The positive cells were enumerated from the two tissue cores and an average density (number of positive cells per mm<sup>2</sup>) was adopted. PD-L1 was scored as positive or negative using a threshold of  $\geq 1$  positive cells in any representative field. The optimal cutoff value of C5aR1 was obtained using the quartile value.

### Peptide blocking experiment

The C5aR1 antibody (Sigma, #HPA014520) was gently mixed with an excess of the corresponding recombinant peptide (Novus, #NBP1-88258PEP), typically at a concentration tenfold that of the antibody. This antibody-peptide mixture was allowed to incubate at room temperature for 1 h. Tissue sections, prepared on slides in accordance with established immunohistochemistry (IHC) protocols as described above, were subsequently subjected to an overnight incubation at 4°C with the pre-incubated antibody solution, both with and without the blocking peptide. Negative controls were treated with PBS. Following this step, the standard staining protocol was uniformly applied to identical sample sets. Staining patterns in sections treated with the C5aR1 antibody alone were systematically compared to those subjected to pre-incubation with the blocking peptide to assess the impact of peptide blocking on the staining outcome.

### Preparation of single cell suspension

Fresh HGSC tissues were collected directly from a patient undergoing surgery or biopsy. The collected tumor tissue is typically transported to the laboratory in a sterile manner on ice to ensure its viability. HGSC tissues were washed with PBS three times, followed by mechanical dissection into small fragments of 1–2 mm<sup>3</sup> size and enzymatic digestion in RPMI-1640 medium containing 1 mg/mL collagenase IV. The dissociated cell suspensions were further incubated for 1 h at 37°C under continuous rotation. The cell suspensions were then filtered through a 100  $\mu$ m cell strainer, washed once with PBS, and resuspended in cell staining buffer.

### Fresh tumor explant cultures

Fresh HGSC tissue ( $n = 36$ ) were promptly processed by manual dissection, yielding human patient-derived tumor fragments (PDTFs) measuring 1–2 mm<sup>3</sup> in size on ice.<sup>16</sup> Subsequently, they were suspended in DMEM (containing 10% FBS, 1% Pen/Strep, and 30 ng/mL of human rIL-2 (Biolegend, #589102)) and then appropriately diluted to achieve a concentration of 8–10 fragments/mL. To facilitate their adherence and growth, these suspended fragments were mixed with 15% Matrigel (Corning, #356234). This suspension, consisting of tumor fragments embedded in Matrigel, was evenly distributed into the wells of 48-well plates at a volume of 40  $\mu$ L per well. Subsequently, the plates were incubated at 37°C to enable proper settling. Following this, 1 mL DMEM containing the respective drugs was introduced into each well. The drugs utilized in the study comprised 10  $\mu$ g/mL anti-PD-1 (Biolegend, #329957) and 1  $\mu$ g/mL PMX53 (R&D Systems, #5473/1). Furthermore, protein transport inhibitor cocktail (eBioscience, #00-4980-93) was introduced during the final 4–6 hours of cell culture. After a culture period of 96 hours from the initial plating, co-cultures were harvested for subsequent analysis via flow cytometry.

### Flow cytometry

Single-cell suspensions were immunostained using a panel of fluorochrome-conjugated monoclonal antibodies (Supplementary Table S3). Samples were blocked with Fc-receptor blocking reagent and incubated with the Zombie Aqua™ Fixable Viability Kit before staining. Samples stained with isotype-matched antibodies were used as negative controls. A Beckman Coulter CytoFLEX flow cytometer was used for sample acquisition, and FlowJo software (version 10.8.1) was used for the analyses.

### Animal experiments

Female B6C3F1 mice (4–5 weeks old) were obtained from Charles River Laboratories. All experiments were performed in accordance with the guidelines for experimental animals at Fudan University of China. OV2944-HM1 cells ( $1 \times 10^6$ ) were subcutaneously injected into the right flank of mice after depilation. The tumor volume (mm<sup>3</sup>) was measured every second day and calculated as  $(\text{length} \times \text{width}^2)/2$ . PMX53 (1 mg/kg) was injected intraperitoneally beginning 2 days after implantation every two days thereafter until the end of the experiment. On the indicated days, tumors were harvested and digested into a single-cell suspension for flow cytometry analysis.

### Single-cell RNA-seq analysis

Single-cell RNA sequencing (scRNA-seq) profiles and clinical information from five independent OV specimens were obtained from Gene Expression Omnibus (GEO, GSE154600). Genes that were expressed in less than three cells and cells that expressed less than 200 genes were excluded. Furthermore, the data were filtered

to include cells that expressed no more than 6000 genes and less than 10% of mitochondrial transcripts. After quality control, 40218 cells were obtained. After data normalization, principal component analysis, and Uniform Manifold Approximation and Projection (UMAP), eight clusters were identified and defined using canonical cell markers. The R package ‘CellChat’ was used to infer intercellular communication networks using a database of interactions among ligands, receptors, and their cofactors.

### External data source and computational analysis

Transcriptomic, mutation, and clinical data from TCGA-OV were downloaded from the GDC Data Portal in Dec 2019. RNA-seq data were normalized to transcripts per million (TPM). The expression data and clinical information of the three ICB-treatment cohorts were downloaded from GEO or public papers. The HPA RNA-Seq data was obtained from Array Express Archive ([www.ebi.ac.uk/arrayexpress/](http://www.ebi.ac.uk/arrayexpress/)) with the accession number: E-MTAB-1733.<sup>17</sup> CAGE peaks expression was obtained from <http://fantom.gsc.riken.jp/5/data>.<sup>18</sup> Gene Set Enrichment Analysis (GSEA) was conducted using the GSEA software (<http://software.broadinstitute.org/gsea/>). The R package ‘limma’ was used to identify differentially expressed genes between the patients with high and low C5aR1 expression. The indicated gene signatures are listed in Supplementary Table S4.

### Statistical analyses

Significant differences between two groups were determined using either the Mann-Whitney U test, unpaired t-test, or paired t-test. Significant differences between three or more groups were determined by one-way ANOVA or two-way ANOVA followed by multiple comparisons using the Bonferroni post hoc test. Simple correlations were summarized using Spearman’s correlation coefficients. Kaplan-Meier analysis and log-rank test were used to analyze the OS of patients with HGSC. Pearson’s chi-square test and Fisher’s exact test were used to compare the variables. Univariate and multivariate analyses were performed using Cox regression survival analyses. All statistical analyses were performed using GraphPad Prism software (version 8.0) and MedCalc software (version 15.2.2). Asterisks indicate the significance level of  $P$  value: \* $P < .05$ , \*\* $P < .01$ , and \*\*\* $P < .001$ . Data are shown as mean  $\pm$  SD.

## Results

### C5aR1 expression associates with unfavorable outcome in HGSC

To investigate the clinical significance of C5aR1 in HGSC, we applied Kaplan-Meier curves and log-rank tests to compare overall survival (OS) between the high and low C5aR1 subgroups. In both Discovery and TCGA cohorts, higher expression of C5aR1 was associated with dismal prognosis (hazard ratio [HR] = 2.790, 95% confidence interval [CI],

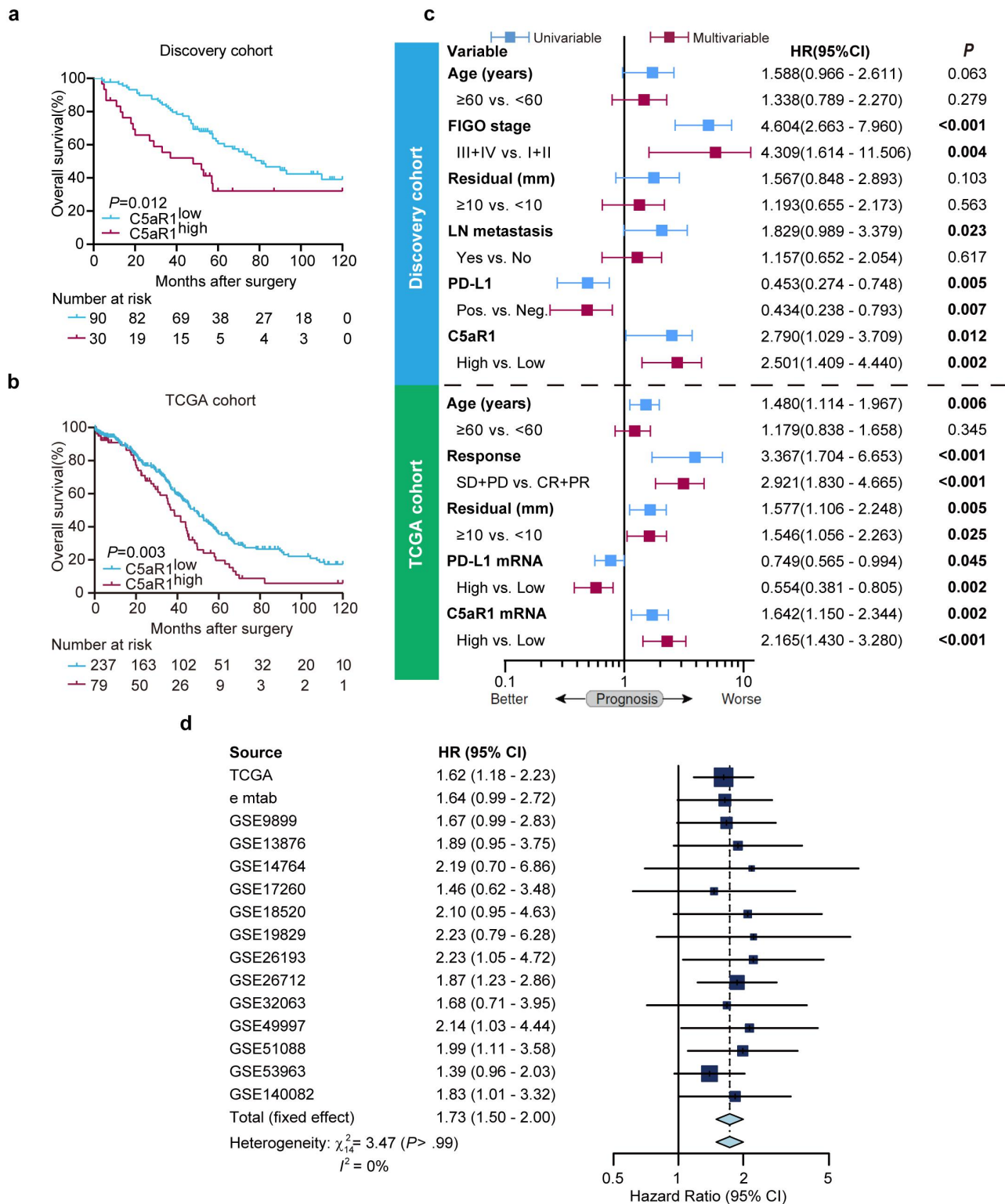


**Figure 1.** C5aR1 expression associates with unfavorable outcome in HGSC. (a,b) Kaplan-Meier curves of overall survival from HGSC patients in the Discovery cohort (A,  $n = 120$ ) and TCGA cohort (B,  $n = 316$ ) that was stratified by high versus low C5aR1 level. (c) Univariate and multivariate cox regression for C5aR1 and clinic-pathological variables in Discovery cohort and TCGA cohort. HR, hazard ratio; CI, confidence interval; LN metastasis, lymph nodes metastasis; Pos., positive; Neg., negative; Significant  $P$  value ( $P < .05$ ) are bolded. (d) Forest plot of meta-analysis evaluating the associations between the C5aR1 expression levels and prognostic indicators in 15 HGSC cohorts.

1.029–3.709,  $P = .012$ , and HR = 1.642, 95%CI, 1.150–2.344,  $P = .002$ , respectively) (Figure 1a,b). Multivariate Cox regression analysis indicated that C5aR1 could be a potential independent prognostic factor for OS in both Discovery and

TCGA cohorts. Consistently, the expression of PD-L1 was associated with favorable prognosis in multivariate analysis (Figure 1c). For a systematic comprehensive evaluation and quantitative analysis, we leveraged the fixed-effects model to

pool multiple independent studies of HGSC. The pooled results indicated that higher C5aR1 expression was associated with poorer prognosis (HR = 1.73, 95% CI:1.50–2.00,  $P < 0.001$ ) (Figure 1d, Supplementary Table S5). In conclusion, higher expression of C5aR1 maybe associated with unfavorable outcomes.

### **C5aR1 expression correlate with immunosuppressive tumor microenvironment in HGSC**

We investigated the role of C5aR1 in the tumor microenvironment, which plays an important role in clinical outcomes and immunotherapy response. Tumor-associated immune cells and effector molecules were evaluated using IHC in the Discovery cohort. First, we used peptide blocking experiment to confirm the specificity of commercial C5aR1 antibody and showed that reduced staining intensity on the peptide-blocked slide compared to anti-C5aR1 antibody-only slide (Supplementary Figure S3A). Furthermore, we explored the data from Human Protein Atlas to validate the correlation between mRNA and protein (staining with the same commercial C5aR1 antibody). There was a strong positive correlation between mRNA and protein levels, it suggested that changes in mRNA expression are likely reflected in protein abundance and further confirmed the specificity of the commercially available anti-C5aR1 antibody (Supplementary Figure S3B-C). As expected, high C5aR1 expression was associated with increased expression of Treg cells, M2-polarized macrophages, neutrophils, IL-10, and TGF- $\beta$  (Figure 2a). Meanwhile, we observed that C5aR1 expression was positively correlated with score of T cell dysfunction signature in the TCGA cohort<sup>19</sup> (Figure 2b). Similarly, tumors with high C5aR1 expression upregulated the expression of signaling pathways involved in the TGF- $\beta$  and IL-10 pathways (Figure 2c). In addition, we investigated the functional phenotype of CD8<sup>+</sup> T cells in the high and low C5aR1 subgroups. Notably, the expression of the effector molecule GZMB was increased, while the immune checkpoints PD-1 and CTLA-4 in CD8<sup>+</sup> T cells were marginally decreased in tumors with high C5aR1 expression. Consistently, tumors with high C5aR1 expression upregulated the expression of TGF- $\beta$  and IL-10, which are immunosuppressive cytokines that promote tumor immune escape and drive immunotherapy resistance.<sup>20,21</sup> Flow cytometry analysis also illustrated that more Tregs and CD206<sup>+</sup> macrophages were present in tumors with high C5aR1 expression, whereas more HLA-DR<sup>+</sup> macrophages were present in counterparts with low C5aR1 expression (Figure 2d). Consistently, we also found a positive correlation between high C5aR1 expression and immune cells, including memory B cells, CD8<sup>+</sup> T cells, follicular helper T cells (T<sub>fh</sub>s), activated NK cells, M2-polarized macrophages, activated mast cells and neutrophils by using the CIBERSORT algorithm (Figure 2e). Altogether, these results suggest that C5aR1 may be associated with the establishment of an immunosuppressive tumor microenvironment.

### **Inhibition of C5aR1 retard tumor growth and reactivate anti-tumor immunity**

To investigate the therapeutic effects of C5aR1 inhibition *in vivo*, HM1 cells were implanted subcutaneously into syngeneic B6C3F1 mice, and PMX53 (a C5aR1 antagonist) was administered beginning 2 days after implantation every two days (Figure 3a). PMX53 significantly altered the tumor growth kinetics and inhibited tumor growth (Figure 3b,c). Treatment with PMX53 led to an increase in the percentage of granzyme B<sup>+</sup>CD8<sup>+</sup>T cells, M1-polarized macrophages, while reduced IL-10<sup>+</sup>Tregs, and PD-1<sup>+</sup>CTLA-4<sup>+</sup>CD8<sup>+</sup>T cells (Figure 3d). Differential expression analysis of PMX53-treated and untreated mice identified 457 significant genes (Benjamini and Hochberg adjusted  $P$  value  $< 0.05$ ,  $\log_2$ (fold change)  $> 0.5$ ) (Supplementary Table S6). A number of immune-related genes downregulated in PMX53-treated mice including chemokines (*Cxcl2* and *Cxcl13*) and critical nodes of the TCR signaling pathway (*Lck*, *Lat* and *Zap70*),<sup>22,23</sup> while apoptotic genes (*Deptor*, *Perp* and *Sfn*) were upregulated in PMX53-treated mice (Figure 3e). Furthermore, we observed decreased expression of mRNAs associated with epithelial-mesenchymal transition, extracellular matrix organization, negative regulation of inflammatory response, and vasculature development in PMX53-treated mice (Figure 3f). To further decipher the effect of PMX53 on the tumor immune microenvironment of HGSC specimens, HGSC fresh tumor explant cultures were generated. The same results were observed after PMX53 treatment in *ex vivo* HGSC models, with elevated percentages of granzyme B<sup>+</sup>CD8<sup>+</sup>T cells and M1-polarized macrophages, and a reduced percentage of PD-1<sup>+</sup>CTLA-4<sup>+</sup>CD8<sup>+</sup>T cells and IL-10<sup>+</sup> Treg cells (Figure 3g). Overall, these data suggest that C5aR1 may be a potential target for reinvigorating anti-tumor immunity by reshaping the immunosuppressive tumor microenvironment of HGSC.

### **Inhibition of C5aR1 enhances the anti-tumor efficacy of anti-PD-1 immunotherapy**

Given that C5aR1 confers to an immunosuppressive tumor microenvironment, we hypothesized that elevated C5aR1 expression might be related to resistance to immune checkpoint blockade therapy (ICB). In line with this hypothesis, C5aR1 expression was positively correlated with two sets of genes, including the tumor immune dysfunction and exclusion (TIDE) framework and the innate anti-PD-1 resistance (IPRES) framework<sup>19,24</sup>(Figure 4a). We further evaluated the clinical significance of C5aR1 expression in immunotherapy in HGSC fresh tumor explant cultures. Compared with HGSC with high C5aR1 expression, anti-PD-1 antibody treatment increased the proportion of granzyme B<sup>+</sup>, IFN- $\gamma$ <sup>+</sup> and double positive (granzyme B<sup>+</sup>IFN- $\gamma$ <sup>+</sup>) CD8<sup>+</sup>T cells in tumors with low C5aR1 expression (Figure 4b). Interestingly, PMX53 synergized with anti-PD-1 antibody therapy by augmenting the cytotoxic activity of CD8<sup>+</sup> T-cells (Figure 4c). Furthermore, we investigated the ability of C5aR1 to predict clinical outcomes in response to ICB therapy in three publicly available ICB-treated cohorts.<sup>25–27</sup> We classified the patients into two

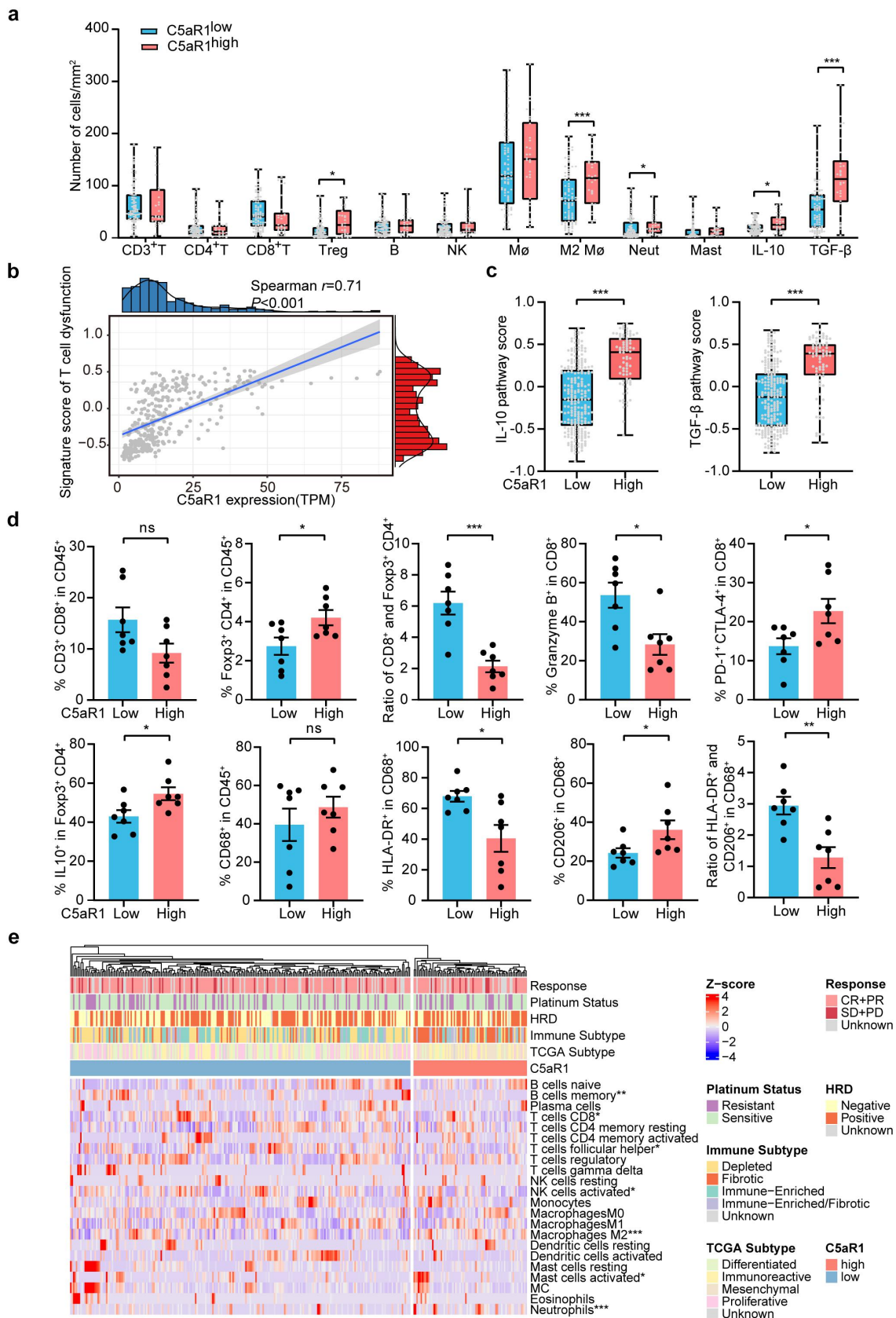


**Figure 2.** C5aR1 expression correlates with immunosuppressive tumor microenvironment in HGSC. (a) Comparison of the indicated immune cells and immune molecules between high ( $n = 30$ ) and low ( $n = 90$ ) C5aR1 groups. Mø, macrophages; M2 Mø, M2-polarized macrophages; Neut, neutrophils; Mast, mast cells. (b) Correlation dot plot between C5aR1 expression and score of T cell dysfunction signature in HGSC specimens of TCGA cohort. Lines with colored field represent the regression line with 95% confidence interval, including histogram and kernel density estimates. (c) Enrichments for the indicated gene signatures IL-10 pathway and TGF- $\beta$  pathway in samples with low C5aR1 expression versus samples with high C5aR1 expression (low,  $n = 237$ ; high,  $n = 79$ ). (d) Proportion of immune cells and immune molecules of HGSC patients with low ( $n = 7$ ) and high ( $n = 7$ ) C5aR1 level. (e) Heatmap displaying normalized immune cell compositions calculated by CIBERSORT and clinicopathologic features (response, platinum status, HRD, immune subtype and TCGA subtype) in C5aR1-stratified clusters in TCGA cohort. CR, complete remission; PR, partial remission; SD, stable disease; PD, progressive disease; HRD, homologous recombination deficiency.

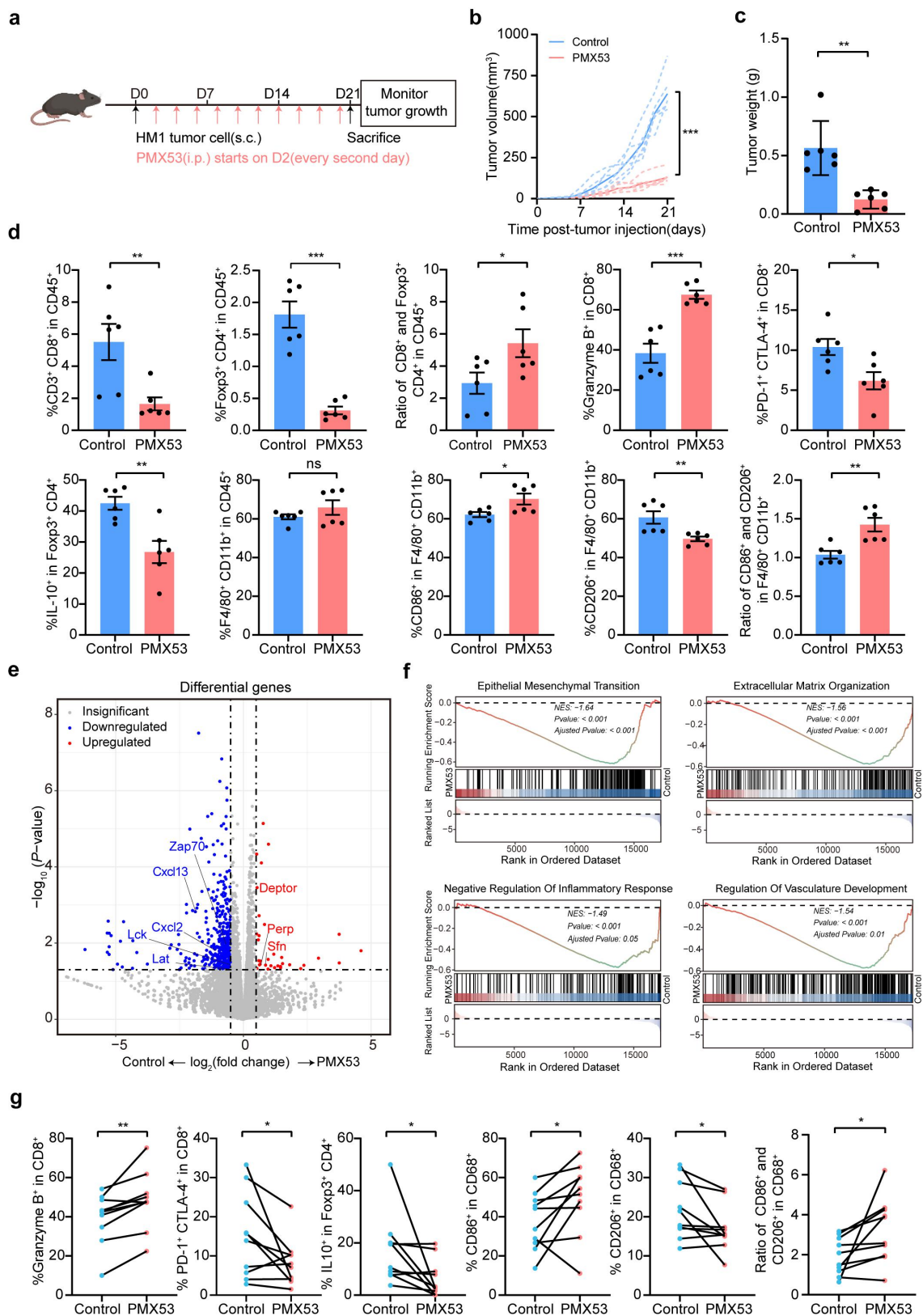


**Figure 3.** Inhibition of C5aR1 retards tumor growth and reactivates anti-tumor immunity. (a) Comparison of the indicated immune cells and immune molecules between high ( $n = 30$ ) and low ( $n = 90$ ) C5aR1 groups. M $\phi$ , macrophages; M2 M $\phi$ , M2-polarized macrophages; Neut, neutrophils; Mast, mast cells. (b) Correlation dot plot between C5aR1 expression and score of T cell dysfunction signature in HGSC specimens of TCGA cohort. Lines with colored field represent the regression line with 95% confidence interval, including histogram and kernel density estimates. (c) Enrichments for the indicated gene signatures IL-10 pathway and TGF- $\beta$  pathway in samples with low C5aR1 expression versus samples with high C5aR1 expression (low,  $n = 237$ ; high,  $n = 79$ ). (d) Proportion of immune cells and immune molecules of HGSC patients with low ( $n = 7$ ) and high ( $n = 7$ ) C5aR1 level. (e) Heatmap displaying normalized immune cell compositions calculated by CIBERSORT and clinicopathologic features (response, platinum status, HRD, immune subtype and TCGA subtype) in C5aR1-stratified clusters in TCGA cohort. CR, complete remission; PR, partial remission; SD, stable disease; PD, progressive disease; HRD, homologous recombination deficiency.

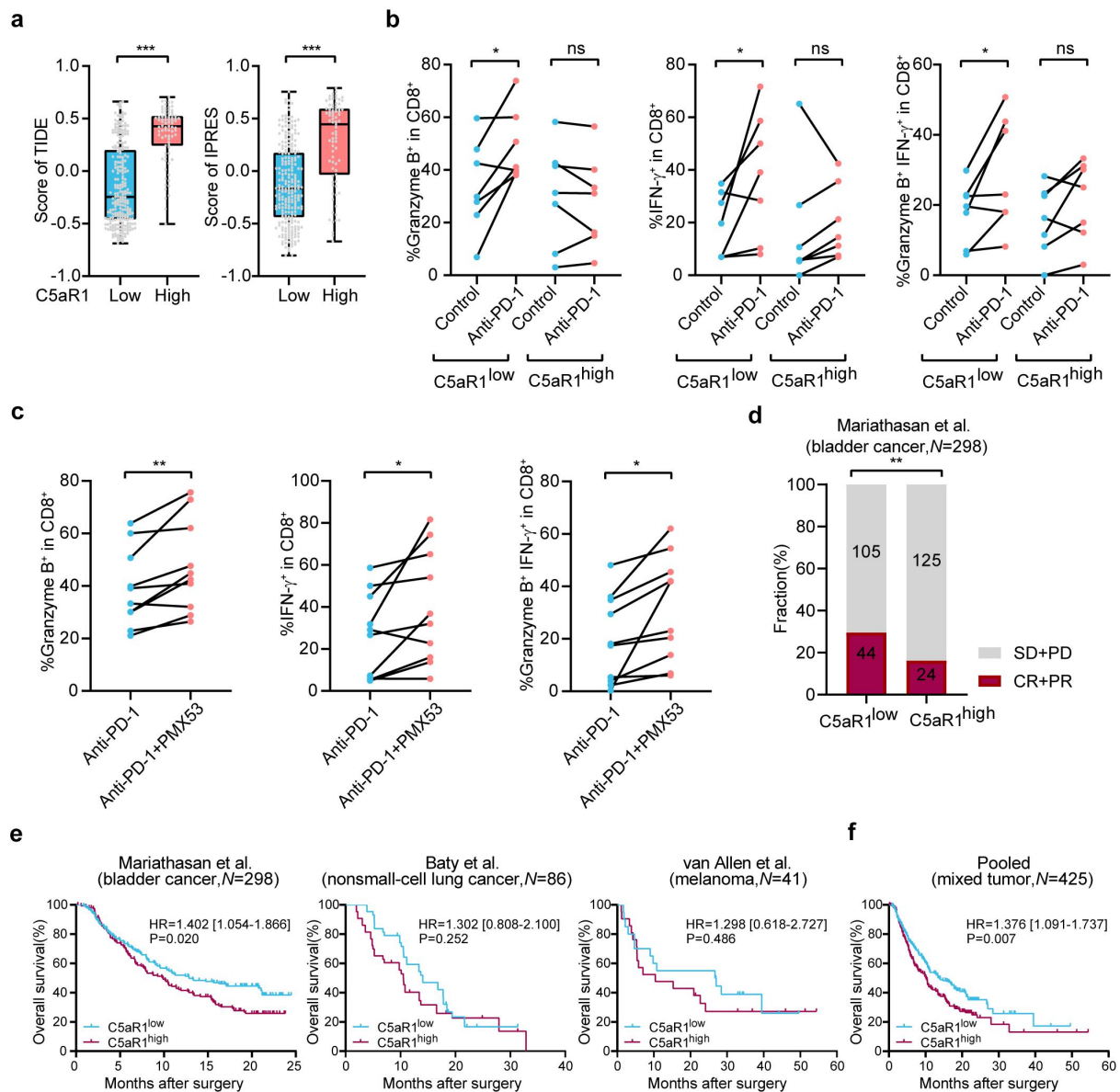


**Figure 4.** Inhibition of C5aR1 enhances the anti-tumor efficacy of anti-PD-1 immunotherapy. (a) Enrichments for IL-10 pathway and TGF- $\beta$  pathway signatures in patients with low and high C5aR1 expression from TCGA cohort. (b) Proportion of GZMB, and IFN- $\gamma$  in CD8<sup>+</sup> T cells of 14 HGSC fresh tumor explant cultures (low,  $n = 7$ ; high,  $n = 7$ ) across control group and anti-PD-1 group. (c) Proportion of GZMB, and IFN- $\gamma$  in CD8<sup>+</sup> T cells of 20 HGSC fresh tumor explant cultures (low,  $n = 10$ ; high,  $n = 10$ ) across anti-PD-1 group and anti-PD-1+PMX53 group. (d) Clinical response to PD-L1 blockade by C5aR1 expression in IMvigor210 cohort. (e and f) The expression of C5aR1 in predicting survival of patients receiving ICB treatment is shown for individual datasets (e) and pooled data (f).

groups based on the median expression of C5aR1. Patients with MIBC failed to respond to anti-PD-1 therapy in tumors with high C5aR1 (Figure 4d). Patients with low C5aR1 expression exhibited favorable survival outcomes to ICB therapy compared with counterparts with high C5aR1 expression, regardless of the tumor type or ICB-containing regimen (HR = 0.71,  $P = .007$  for pooled cohort) (Figure 4w,f). C5aR1 may be useful as a marker of the clinical benefit of ICB therapy and as a potential therapeutic target for enhanced ICB sensitivity.

### **C5aR1 is mainly expressed on macrophages and contributes to immunosuppressive phenotype**

To examine the cellular source of C5aR1, we analyzed publicly available scRNA-seq data from five biopsies from HGSC.<sup>28</sup>

After quality control and exclusion of batch effects, 40218 single cells were analyzed and clustered into eight populations (Figure 5a). Using cell-specific markers, we identified five immune cell types, namely T cells, myeloid cells, plasma cells, B cells, and plasmacytoid dendritic cells (pDC), as well as three nonimmune cell types (epithelial cells, fibroblasts, and endothelial cells) (Figure 5b). Myeloid cells were analyzed separately and further grouped into four sub-clusters (macrophages, monocytes, cycling, and dendritic cells). Remarkably, C5aR1 expression was specifically confined to myeloid cells, especially in macrophages and monocytes (Figure 5c), which was consistent with the co-expression of C5aR1 and CD68 observed by immunofluorescence (Supplementary Figure S4A-B). C5aR1 was barely or rarely expressed in tumor cells which belongs to clusters of epithelial cells. By creating



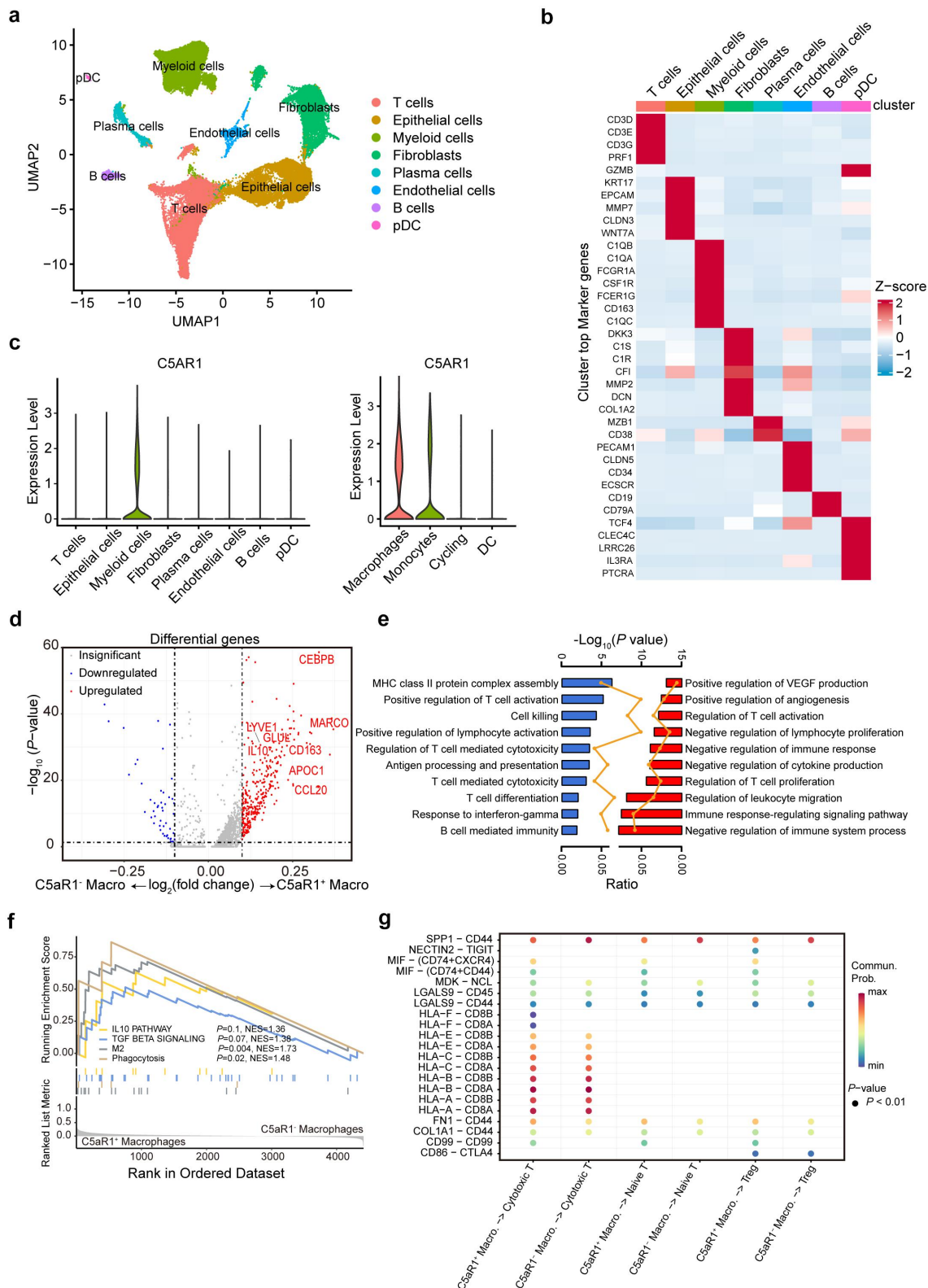


**Figure 5.** C5aR1 is mainly expressed on macrophages and contributes to immunosuppressive phenotype. (a) The UMAP plot visualizes cell clusters ( $n = 8$ ) in HGSC profiled by scRNA-seq. (b) Heatmap of Z-score expression of canonical cell markers of each immune cell population. (c) Violin plots showing C5aR1 mRNA expression across all clusters (left) and myeloid cell sub-clusters (right). (d) Volcano plot showing differentially expressed genes ( $\log_2(\text{fold change}) > 0.5$ ,  $P$  value  $< .05$ ) upregulated (right) or downregulated (left) in C5aR1<sup>+</sup> macrophages versus C5aR1<sup>-</sup> macrophages. (e) Gene set enrichment analysis based on differentially expressed genes (blue: downregulated pathways; red: upregulated pathways in C5aR1<sup>+</sup> macrophages). The bar chart represents the significance of the gene enrichment for any given pathway. The orange lines indicate the ratio or percentage coverage of a pathway subject to pathway size bias. (f) Gene set enrichment analysis (GSEA) plot showing the enrichment scores for the IL-10, TGF- $\beta$ , M2 polarization, and phagocytosis pathways in C5aR1<sup>+</sup> macrophages. (g) Bubble plot showing inferred ligand-receptor pairs between C5aR1<sup>+</sup> macrophages or C5aR1<sup>-</sup> macrophages and T cells from scRNA-seq using CellChat. The depth of color from blue to red represents the low to high communication probability. The sizes of the bubbles represent the corresponding  $P$  value. Commun. Prob: Communication probability.

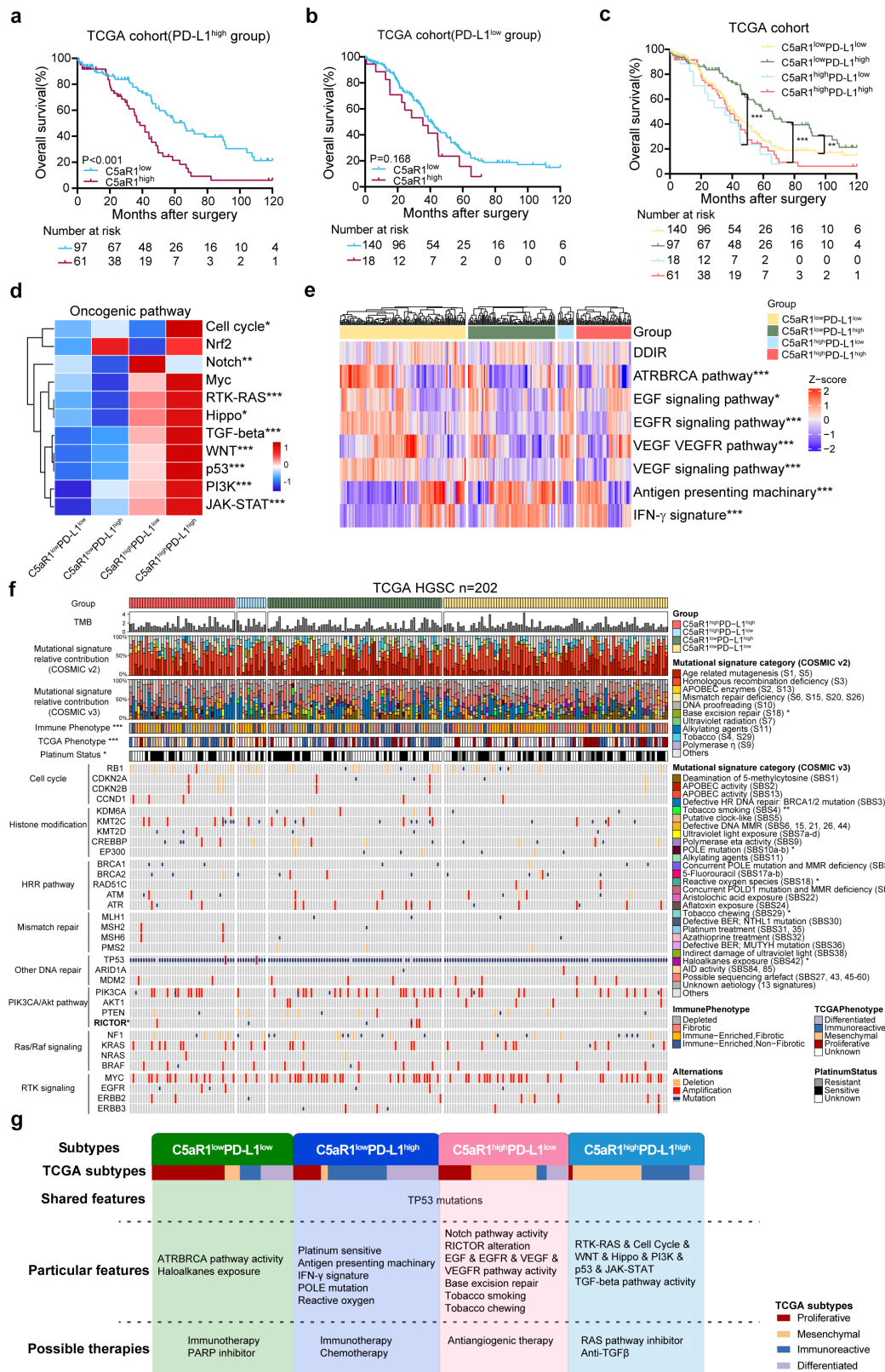


**Figure 6.** C5aR1 and PD-L1 expression panel correlates with oncogenic pathway activity, therapeutic signatures and molecular alterations. (a,b) Kaplan-Meier curves of OS in HGSC patients with high PD-L1 levels (A,  $n = 158$ ) or low PD-L1 levels (B,  $n = 158$ ) from TCGA. (c) Kaplan-Meier analyses of OS in TCGA patients stratified according to the combination of C5aR1 and PD-L1. (d) Oncogenic pathway activity across the C5aR1 and PD-L1 expression panels. Pathway activity was estimated as the mean expression of downstream genes targeted by each pathway. (e) Heatmap displaying the scores of therapy-related signatures (calculated using GSVA). Samples were ordered by unsupervised hierarchical clustering, and the scale represented Z-score normalization. (f) The genomic landscape of 202 high-grade serous ovarian cancers stratified according to the combination of C5aR1 and PD-L1. The genomic features are displayed from top to bottom as follows: subtype, genome-wide tumor mutational burden (TMB), relative contribution of mutational signatures via COSMIC ver2 and ver3, immune phenotype, TCGA phenotype, platinum status, and an overview of significantly mutated genes. (g) Summary of molecular characteristics found in the present study and potential therapeutic implications for the treatment of high-grade serous ovarian cancer per C5aR1 and PD-L1 expression panel subtype.

histograms to visualize the distribution of C5aR1 expression on different cell types, calculating mean fluorescence intensity (MFI) and analyzing the data statistically, we confirmed the predominant expression on macrophages, neutrophils and monocytes, rather than T cells and tumor cells (Supplementary Figure S4C). Analysis of differentially expressed genes indicated that *Il10*, *CD163* and *Ccl20* were upregulated in C5aR1<sup>+</sup> macrophages (Figure 5d). Gene Ontology (GO) term enrichment analysis of DEGs revealed that in addition to the negative regulation of lymphocyte proliferation, immune response, and cytokine production to reshape the immune microenvironment, C5aR1<sup>+</sup> macrophages also have the potential to positively regulate VEGF production and angiogenesis (Figure 5e). Consistently, gene set enrichment analysis (GSEA) demonstrated that upregulated genes in C5aR1<sup>+</sup> macrophages were enriched in the IL-10 pathway, TGF- $\beta$  signaling, M2 polarization, and phagocytosis, indicating an immunosuppressive phenotype (Figure 5f). In addition, C5aR1<sup>+</sup> macrophages were predicted to interact with cytotoxic CD8<sup>+</sup> T cells and naïve CD8<sup>+</sup>T cells via the MIF-(CD74 +CXCR4) and MIF-(CD74+CD44) axes, suggesting that C5aR1<sup>+</sup> macrophages could regulate the proliferation and effector function of CD8<sup>+</sup> T cells.<sup>29,30</sup> C5aR1<sup>+</sup> macrophages were inferred to interact with Treg cells via the NECTIN2-TIGIT axis, which is reported to promote the immunosuppressive function of Treg cells in HGSC.<sup>31,32</sup> These data suggest that tumor-associated macrophages (TAMs) are the main cellular source of C5aR1 and contribute to the immunosuppressive microenvironment of HGSC.

### **C5aR1 and PD-L1 expression panel correlates with oncogenic pathway activity, therapeutic signatures and molecular alterations**

Since both C5aR1 and PD-L1 expression are independent prognostic factors of OS in HGSC (Figure 1c), we hypothesized that the combination of C5aR1 and PD-L1 could improve the predictability of OS and response to targeted treatment in HGSC. We observed a positive correlation between C5aR1 and PD-L1 expression at the mRNA level (Figure 6a). In addition, the analysis of hazard curves for C5aR1 according to PD-L1 expression status showed a negative correlation between high C5aR1 expression and OS in subgroups with PD-L1 expression levels above the median (Figure 6b). Survival analysis confirmed prolonged survival outcomes in the C5aR1<sup>low</sup>PD-L1<sup>high</sup> subgroup (Figure 6c). To characterize the activity of the oncogenic pathway at the expression level, we evaluated pathway activities by calculating the expression value of genes involved in the pathway for each tumor (Figure 6d). Oncogenic pathways, including RTK-RAS, cell cycle, WNT, Hippo, PI3K, p53, JAK-STAT, and TGF- $\beta$  signaling, were increased in the C5aR1<sup>high</sup>PD-L1<sup>high</sup> subgroup, while Notch signaling was increased in the C5aR1<sup>high</sup>PD-L1<sup>low</sup> subgroup<sup>33</sup> (Figure 6d). Next, we dissected the therapeutic signatures composed of the genes most frequently used to infer treatment (Figure 6e). The C5aR1<sup>low</sup>PD-L1<sup>low</sup> subgroup was enriched for ATRBRCA pathway signaling, while the C5aR1<sup>high</sup>PD-L1<sup>low</sup> subgroup was enriched for EGF, EGFR, VEGF, and VEGFR signaling. A high signature score of IFN- $\gamma$  indicated that short-

term IFN- $\gamma$  stimulation can further upregulate antigen presentation activity,<sup>34,35</sup> which may explain the possible mechanism of favorable prognosis in the C5aR1<sup>low</sup>PD-L1<sup>high</sup> subgroup (Figure 6e). To elucidate the molecular landscape, we conducted a comprehensive transcriptomic and genomic analysis of HGSC (Figure 6f). The C5aR1<sup>high</sup>PD-L1<sup>high</sup> subgroup displays a mesenchymal phenotype related to migration and invasion. In contrast, the C5aR1<sup>low</sup>PD-L1<sup>high</sup> subgroup exhibited an immunoreactive phenotype, with better clinical outcomes.<sup>36</sup> The C5aR1<sup>low</sup>PD-L1<sup>high</sup> subgroup was enriched in patients previously identified as platinum-sensitive. The C5aR1<sup>high</sup>PD-L1<sup>low</sup> subgroup showed a higher rate of RICTOR DNA alterations than the other subtypes, which would confer aberrant activity to the mTORC2 pathway.<sup>37</sup> Finally, we assessed the clinical relevance of the transcriptomic characteristics and genomic alterations and described the rationale for therapeutic options for patients with HGSC (Figure 6g). Tumors of the C5aR1<sup>low</sup>PD-L1<sup>low</sup> subtype could benefit from immunotherapy or PARP inhibitors, whereas the C5aR1<sup>low</sup>PD-L1<sup>high</sup> subtype might be susceptible to immunotherapy or chemotherapy. Subtype C5aR1<sup>high</sup>PD-L1<sup>low</sup> may be sensitive to anti-angiogenic targeted therapies. The C5aR1<sup>high</sup>PD-L1<sup>high</sup> subtype could benefit from RAS pathway inhibitors or TGF- $\beta$  inhibitors. Overall, the HGSC classification based on C5aR1 and PD-L1 panels deserves further evaluation for precision targeted therapy.

## **Discussion**

The emerging use of complement inhibitors, specifically C3 blockers, in combination with checkpoint inhibitors, has garnered significant interest in the field of ovarian cancer treatment. Ovarian cancer is notorious for its ability to evade the immune system through various mechanisms, including the dysregulation of the complement system and immune checkpoint pathways. Recent research suggests that combining complement blockers with checkpoint inhibitors could offer a promising strategy to enhance the immune response against ovarian cancer cells.<sup>38</sup>

Complement inhibitors targeting the C3 protein have shown potential in modulating the tumor microenvironment by disrupting the complement cascade, which is often exploited by cancer cells to establish an immunosuppressive milieu.<sup>39</sup> One ongoing clinical trial that pertains to this combination therapy is NCT04919629.<sup>40</sup> This trial likely seeks to investigate the safety, efficacy, and overall potential of combining a C3 blocker with checkpoint inhibitors in treating ovarian cancer. The trial's results could provide valuable insights into the feasibility of this novel therapeutic approach, shedding light on its effectiveness, potential side effects, and patient outcomes. It's important to note that the success of such a combination therapy could revolutionize ovarian cancer treatment and offer new hope for patients facing this challenging disease.

Accumulating evidence suggests that the complement system is a major regulator of the tumor microenvironment. Complement seems to mediate evasion of the immune system to remodel the tumor microenvironment and facilitate tumor progression.<sup>41,42</sup> In this study, we provide a framework for the

evaluation of C5aR1. First, high-level expression in HGSC predicts unsatisfactory overall survival. Second, it implies an immunosuppressive tumor microenvironment. Third, we delivered marked anti-tumor immune responses and an innovative combination strategy in which anti-PD-1 antibodies are administered in combination with a C5aR1 inhibitor, and finally, guide individualized targeted therapy and optimize patient selection based on C5aR1 and PD-L1 expression panels.

We identified that C5aR1 contributes to the immunosuppressive tumor microenvironment characterized by high infiltration of Tregs and M2-polarized macrophages. Our data indicate that C5aR1 stabilizes Foxp3 expression and upregulates immunosuppressive Treg activity with elevated IL-10 levels. Moreover, C5aR1 activation allows TGF- $\beta$  to drive the differentiation of CD4<sup>+</sup>T cells toward a Treg phenotype, similar to the effect of high-concentration stimulation of C5a.<sup>43</sup> However, it has also been reported that C5aR1 activation downregulates the levels of Foxp3,<sup>44</sup> suggesting that the role of C5aR1 in stability of Treg may be context-dependent. Based on gene expression abundance at single-cell resolution and protein localization by immunofluorescence, C5aR1 was found to be preferentially expressed in macrophages. C5aR1<sup>+</sup> macrophages exhibit a phenotype similar to that of M2-polarized macrophages, which facilitates immunosuppressive effects through interactions with CD8<sup>+</sup> T cells and Tregs. Furthermore, C5aR1 expression on non-macrophage cells extends its role beyond macrophage-mediated immune responses. Its presence on neutrophils, monocytes and even tumor cells underscore its significance in inflammation, immunity, and disease.<sup>45–47</sup> Understanding the diverse roles of C5aR1 in different cell types is a dynamic area of research with the potential to yield novel therapeutic interventions. Therefore, a comprehensive understanding of the effects of C5aR1 on the tumor microenvironment could help develop novel targeting strategies and combine existing therapies to improve patient survival outcomes.

Experimental data also indicated a regulatory effect of C5aR1 on CD8<sup>+</sup>T cell biology. Patients with ovarian cancer with high C5aR1 expression acquire an immunosuppressive phenotype by restraining CD8<sup>+</sup> T cell proliferation and impairing granzyme B production. As expected, the therapeutic effect of C5aR1 blockade was accompanied by an increase in the expression of effector molecules and a decrease in the expression of exhaustion markers by CD8<sup>+</sup> T cells. Interestingly, a decreased frequency of CD8<sup>+</sup> T cells was observed in PMX53-treated mice, suggesting that CD8<sup>+</sup> T cell quality, rather than quantity, determined anti-tumor immunity efficacy. The clinical success of immune checkpoint blockade therapy is primarily attributed to the reinvigoration of tumor antigen – specific T cells,<sup>48</sup> highlighting the importance of T cell functionality. The results obtained in fresh tumor explant cultures suggest that blocking C5aR1 enhances the clinical efficacy of anti-PD-1 therapy. The most plausible explanation for this synergism is that C5aR1 signaling hampers the anti-tumor activity of anti-PD-1 antibodies. In agreement with this hypothesis, our data showed that the combined treatment led to increased expression of granzyme B and IFN- $\gamma$  in CD8<sup>+</sup> T cells, which suggests a more complete

restoration of CD8<sup>+</sup> T cell effector functions. These studies suggest that C5aR1 blockade, in combination with other immunotherapies, may provide substantial benefits for patients who do not respond adequately to a single ICB agent. Manipulating C5aR1 regulation in HGSC is a prospect that, to our knowledge, is yet to be pursued and could represent a new immunotherapeutic to be used in tandem with ICB to improve patient outcomes.

Another scenario in which C5aR1 may be of clinical relevance is to guide the identification of potential therapeutic targets in combination with PD-L1. The management of ovarian cancer has evolved from a one-size-fits-all approach to a more precise approach that integrates optimal surgery and systemic therapy with subtype specificity. Standard practice now takes histology, stage, residual status, and genomic profile into account.<sup>49</sup> In the present study, we demonstrated considerable molecular heterogeneity at both the transcriptional and genomic levels in C5aR1 and PD-L1 panel subgroups. Most oncogenic pathways involved in HGSC are activated in the C5aR1<sup>high</sup>PD-L1<sup>high</sup> subgroup, suggesting the substantial potential of clinical trials for associated pathway inhibitor treatment. Bevacizumab and PARP inhibitors have demonstrated significant improvements in some patients undergoing first-line therapy and can be selected for the management of the C5aR1<sup>high</sup>PD-L1<sup>low</sup> and C5aR1<sup>low</sup>PD-L1<sup>low</sup> subgroups, respectively.<sup>50,51</sup> WGS analyses confirmed that mutations in TP53 are a nearly universal characteristic of HGSC among subgroups,<sup>52</sup> while RICTOR alternation identifies the C5aR1<sup>high</sup>PD-L1<sup>high</sup> subgroup and predicts response to drugs targeting mTOR. Therefore, the integrated analysis refines the treatment of HGSC precision tailored to individual predictive factors.

However, it's crucial to interpret these developments within the broader context of clinical research. While the preliminary evidence and rationale for combining complement blockers with checkpoint inhibitors in ovarian cancer are promising, the results of ongoing clinical trials like NCT04919629 will determine the true clinical value of this approach. Additionally, factors such as patient selection, dosing regimens, and potential interactions between the two classes of inhibitors will need to be carefully considered to optimize therapeutic outcomes.

Taken together, the results presented herein provide evidence that C5aR1 is a regulator of ovarian carcinogenesis by promoting an immunosuppressive tumor microenvironment. Our preclinical data demonstrated that therapeutic inhibition of C5aR1 results in the reprogramming of macrophages and reinvigoration of CD8<sup>+</sup> T cells that offset resistance to anti-PD-1 treatment. By identifying particular features based on disease biology and genomic landscape and proposing corresponding potential therapies, novel therapeutic opportunities could be conferred to patients with HGSC.

## Acknowledgments

This work was supported by the Shanghai Key Laboratory of Female Reproductive Endocrine Related Diseases, the Obstetrics and Gynecology Hospital, Fudan University, and Shanghai Cancer Center, Fudan University.

## Disclosure statement

No potential conflict of interest was reported by the author(s).

## Funding

This study was funded by the National Natural Science Foundation of China grants 82072881 (HO Liu), 82273205 (HO Liu), and 82203665 (GD Zhang); Natural Science Foundation of Shanghai grant 20ZR1409000 (HO Liu); Shanghai Sailing Program grant 21YF1403900 (GD Zhang); Foundation of Science and Technology Commission of Shanghai Municipality 22Y31900502 (Y Huang); Shanghai Clinical Research Center for Gynecological Disease 22M1940200 (HO Liu); and Shanghai Urogenital System Disease Research Center 2022ZZ01012 (HO Liu). All study sponsors have no role in the study design, collection, analysis, and interpretation of data.

## ORCID

Haiou Liu  <http://orcid.org/0000-0003-0200-8981>

## Authors' contributions

H.L. performed the study concept, design and acquisition; H.L., Y.H. and G.Z. obtained funding and study supervision; C.Z. and K.C. performed acquisition, analysis, and interpretation of data, and statistical analysis; J. L., M.Y., Y.W., and M.H. provided technical and material support; and all authors read and approved the final manuscript.

## Data availability statement

The datasets used and/or analyzed during the current study are available from the corresponding author upon reasonable request. ScRNA-seq data for this article can be accessed online at <https://www.ncbi.nlm.nih.gov/geo/query/acc.cgi?acc=GSE154600>.

## References

- Disis ML, Taylor MH, Kelly K, Beck JT, Gordon M, Moore KM, Patel MR, Chaves J, Park H, Mita AC, et al. Efficacy and safety of avelumab for patients with recurrent or refractory ovarian cancer: phase 1b results from the JAVELIN solid tumor trial. *JAMA Oncol.* 2019;5(3):393–401. doi:10.1001/jamaoncol.2018.6258.
- Matulonis UA, Shapira-Frommer R, Santin AD, Lisysanskaya AS, Pignata S, Vergote I, Raspagliesi F, Sonke GS, Birrer M, Provencher DM, et al. Antitumor activity and safety of pembrolizumab in patients with advanced recurrent ovarian cancer: results from the phase II KEYNOTE-100 study. *Ann Oncol.* 2019;30(7):1080–1087. doi:10.1093/annonc/mdz135.
- Anadon CM, Yu X, Hänggi K, Biswas S, Chaurio RA, Martin A, Payne KK, Mandal G, Innamarato P, Harro CM, et al. Ovarian cancer immunogenicity is governed by a narrow subset of progenitor tissue-resident memory T cells. *Cancer Cell.* 2022;40(5):545–557. doi:10.1016/j.ccell.2022.03.008.
- Melero I, Berman DM, Aznar MA, Korman AJ, Gracia JLP, Haanen J. Evolving synergistic combinations of targeted immunotherapies to combat cancer. *Nat Rev Cancer.* 2015;15(8):457–472. doi:10.1038/nrc3973.
- Klos A, Tenner AJ, Johswich K-O, Ager RR, Reis ES, Köhl J. The role of the anaphylatoxins in health and disease. *Mol Immunol.* 2009;46(14):2753–2766. doi:10.1016/j.molimm.2009.04.027.
- Markiewski MM, DeAngelis RA, Benencia F, Ricklin-Lichtsteiner SK, Koutoulaki A, Gerard C, Coukos G, Lambris JD. Modulation of the antitumor immune response by complement. *Nat Immunol.* 2008;9(11):1225–1235. doi:10.1038/ni.1655.
- Cavaillon JM, Fitting C, Haeflencavaillon N. Recombinant C5a enhances interleukin-1 and tumor-necrosis-factor release by lipopolysaccharide-stimulated monocytes and macrophages. *Eur J Immunol.* 1990;20(2):253–257. doi:10.1002/eji.1830200204.
- Corrales L, Ajona D, Rafail S, Lasarte JJ, Riezu-Boj JJ, Lambris JD, Rouzaut A, Pajares MJ, Montuenga LM, Pio R, et al. Anaphylatoxin C5a creates a favorable microenvironment for lung cancer progression. *J Immunol.* 2012;189(9):4674–4683. doi:10.4049/jimmunol.1201654.
- Fusakio ME, Mohammed JP, Laumonier Y, Hoebe K, Köhl J, Mattner J. C5a regulates NKT and NK cell functions in sepsis. *J Immunol.* 2011;187(11):5805–5812. doi:10.4049/jimmunol.1100338.
- Gu J, Ding J-Y, Lu C-L, Lin Z-W, Chu Y-W, Zhao G-Y, Guo J, Ge D. Overexpression of CD88 predicts poor prognosis in non-small-cell lung cancer. *Lung Cancer.* 2013;81(2):259–265. doi:10.1016/j.lungcan.2013.04.020.
- Imamura T, Yamamoto-Ibusuki M, Sueta A, Kubo T, Irie A, Kikuchi K, Kariu T, Iwase H. Influence of the C5a–C5a receptor system on breast cancer progression and patient prognosis. *Breast Cancer-Tokyo.* 2016;23(6):876–885. doi:10.1007/s12282-015-0654-3.
- Kaida T, Nitta H, Kitano Y, Yamamura K, Arima K, Izumi D, Higashi T, Kurashige J, Imai K, Hayashi H, et al. C5a receptor (CD88) promotes motility and invasiveness of gastric cancer by activating RhoA. *Oncotarget.* 2016;7(51):84798–84809. doi:10.18632/oncotarget.12656.
- Hu WH, Hu Z, Shen X, Dong L-Y, Zhou W-Z, Yu X-X. C5a receptor enhances hepatocellular carcinoma cell invasiveness via activating ERK1/2-mediated epithelial–mesenchymal transition. *Exp Mol Pathol.* 2016;100(1):101–108. doi:10.1016/j.yexmp.2015.10.001.
- Wada Y, Maeda Y, Kubo T, Kikuchi K, Eto M, Imamura T. C5a receptor expression is associated with poor prognosis in urothelial cell carcinoma patients treated with radical cystectomy or nephroureterectomy. *Oncol Lett.* 2016;12(5):3995–4000. doi:10.3892/ol.2016.5137.
- Maeda Y, Kawano Y, Wada Y, Yatsuda J, Motoshima T, Murakami Y, Kikuchi K, Imamura T, Eto M. C5aR is frequently expressed in metastatic renal cell carcinoma and plays a crucial role in cell invasion via the ERK and PI3 kinase pathways. *Oncol Rep.* 2015;33(4):1844–1850. doi:10.3892/or.2015.3800.
- Cao K, Zhang G, Yang M, Wang Y, He M, Zhang C, Huang Y, Lu J, Liu H. Attenuation of sialylation augments antitumor immunity and improves response to immunotherapy in ovarian cancer. *Cancer Res.* 2023;83(13):2171–2186. doi:10.1158/0008-5472.CAN-22-3260.
- Fagerberg L, Hallström BM, Oksvold P, Kampf C, Djureinovic D, Odeberg J, Habuka M, Tahmasebpour S, Danielsson A, Edlund K, et al. Analysis of the human tissue-specific expression by genome-wide integration of transcriptomics and antibody-based proteomics. *Molecular & Cellular Proteomics: MCP.* 2014;13(2):397–406. doi:10.1074/mcp.M113.035600.
- Forrest ARR, Kawaji H, Rehli M, Baillie JK, de Hoon MJL, Haberle V, Lassmann T, Kulakovskiy IV, Lizio M, Itoh M, et al. A promoter-level mammalian expression atlas. *Nature.* 2014;507:462–470. doi:10.1038/nature13182.
- Jiang P, Gu S, Pan D, Fu J, Sahu A, Hu X, Li Z, Traugh N, Bu X, Li B, et al. Signatures of T cell dysfunction and exclusion predict cancer immunotherapy response. *Nat Med.* 2018;24(10):1550–1558. doi:10.1038/s41591-018-0136-1.
- Connolly EC, Freimuth J, Akhurst RJ. Complexities of TGF- $\beta$  targeted cancer therapy. *Int J Biol Sci.* 2012;8(7):964–978. doi:10.7150/ijbs.4564.
- Emmerich J, Mumm JB, Chan IH, LaFace D, Truong H, McClanahan T, Gorman DM, Oft M. IL-10 directly activates and expands tumor-resident CD8+ T cells without De novo infiltration from secondary lymphoid organs. *Cancer Res.* 2012;72(14):3570–3581. doi:10.1158/0008-5472.CAN-12-0721.
- Poltorak M, Arndt B, Kowtharapu BS, Reddycherla AV, Witte V, Lindquist JA, Schraven B, Simeoni L. TCR activation kinetics and feedback regulation in primary human T cells. *Cell Commun Signal.* 2013;11(1). doi:10.1186/1478-811X-11-4.

23. Acuto O, Di Bartolo V, Michel F. Tailoring T-cell receptor signals by proximal negative feedback mechanisms. *Nat Rev Immunol.* 2008;8(9):699–712. doi:10.1038/nri2397.
24. Hugo W, Zaretsky JM, Sun L, Song C, Moreno BH, Hu-Lieskovan S, Berent-Maoz B, Pang J, Chmielowski B, Cherry G, et al. Genomic and transcriptomic features of response to anti-PD-1 therapy in metastatic melanoma. *Cell.* 2016;165(1):35–44. doi:10.1016/j.cell.2016.02.065.
25. Mariathasan S, Turley SJ, Nickles D, Castiglioni A, Yuen K, Wang Y, Kadel III EE, Koeppen H, Astarita JL, Cubas R, et al. TGF $\beta$  attenuates tumour response to PD-L1 blockade by contributing to exclusion of T cells. *Nature.* 2018;554(7693):544–548. doi:10.1038/nature25501.
26. Baty F, Joerger M, Früh M, Klingbiel D, Zappa F, Brutsche M. 24h-gene variation effect of combined bevacizumab/erlotinib in advanced non-squamous non-small cell lung cancer using exon array blood profiling. *J Transl Med.* 2017;15(1):66. doi:10.1186/s12967-017-1174-z.
27. Van Allen EM. Genomic correlates of response to CTLA-4 blockade in metastatic melanoma (vol 352, aaf8264, 2016). *Science.* 2016;353:229–229.
28. Geistlinger L, Oh S, Ramos M, Schiffer L, LaRue RS, Henzler CM, Munro SA, Daughters C, Nelson AC, Winterhoff BJ, et al. Multiomic analysis of subtype evolution and heterogeneity in high-grade serous ovarian carcinoma. *Cancer Res.* 2020;80(20):4335–4345. doi:10.1158/0008-5472.CAN-20-0521.
29. Simpson KD, Templeton DJ, Cross JV. Macrophage migration inhibitory factor promotes tumor growth and metastasis by inducing myeloid-derived suppressor cells in the tumor microenvironment. *J Immunol.* 2012;189(12):5533–5540. doi:10.4049/jimmunol.1201161.
30. Simpson KD, Cross JV. MIF: metastasis/MDSC-inducing factor? *Oncoimmunology.* 2013;2(3):e23337. doi:10.4161/onci.23337.
31. Chauvin JM, Zarour HM. TIGIT in cancer immunotherapy. *J Immunother Cancer.* 2020;8(2):e000957. doi:10.1136/jitc-2020-000957.
32. Joller N, Lozano E, Burkett P, Patel B, Xiao S, Zhu C, Xia J, Tan T, Sefik E, Jaynik V, et al. Treg cells expressing the coinhibitory molecule TIGIT selectively inhibit proinflammatory Th1 and Th17 cell responses. *Immunity.* 2014;40(4):569–581. doi:10.1016/j.immuni.2014.02.012.
33. Nakauma-Gonzalez JA, Rijnders M, van Riet J, van der Heijden MS, Voortman J, Cuppen E, Mehra N, van Wilpe S, Oosting SF, Rijstenberg LL, et al. Comprehensive molecular characterization reveals genomic and transcriptomic subtypes of metastatic urothelial carcinoma. *Eur Urol.* 2022;81(4):331–336. doi:10.1016/j.eururo.2022.01.026.
34. Ayers M, Luceford J, Nebozhyn M, Murphy E, Loboda A, Kaufman DR, Albright A, Cheng JD, Kang SP, Shankaran V, et al. IFN- $\gamma$ -related mRNA profile predicts clinical response to PD-1 blockade. *J Clin Invest.* 2017;127(8):2930–2940. doi:10.1172/JCI91190.
35. Senbabaoglu Y, Gejman RS, Winer AG, Liu M, Van Allen EM, de Velasco G, Miao D, Ostrovskaya I, Drill E, Luna A, et al. Tumor immune microenvironment characterization in clear cell renal cell carcinoma identifies prognostic and immunotherapeutically relevant messenger RNA signatures. *Genome Biol.* 2016;17(1):231. doi:10.1186/s13059-016-1092-z.
36. Tothill RW, Tinker AV, George J, Brown R, Fox SB, Lade S, Johnson DS, Trivett MK, Etemadmoghadam D, Locandro B, et al. Novel molecular subtypes of serous and endometrioid ovarian cancer linked to clinical outcome. *Clin Cancer Res.* 2008;14(16):5198–5208. doi:10.1158/1078-0432.CCR-08-0196.
37. Cheng HY, Zou Y, Ross JS, Wang K, Liu X, Halmos B, Ali SM, Liu H, Verma A, Montagna C, et al. RICTOR amplification defines a novel subset of patients with lung cancer who May benefit from treatment with mTORC1/2 inhibitors. *Cancer Discov.* 2015;5(12):1262–1270. doi:10.1158/2159-8290.CD-14-0971.
38. Reis ES, Mastellos DC, Ricklin D, Mantovani A, Lambris JD. Complement in cancer: untangling an intricate relationship. *Nat Rev Immunol.* 2018;18(1):5–18. doi:10.1038/nri.2017.97.
39. Ricklin D, Hajishengallis G, Yang K, Lambris JD. Complement: a key system for immune surveillance and homeostasis. *Nat Immunol.* 2010;11(9):785–797. doi:10.1038/ni.1923.
40. ClinicalTrials.gov. *Randomized Phase 2 Trial Of APL-2 With Pembrolizumab Vs. APL-2 With Pembrolizumab And Bevacizumab vs. Bevacizumab Alone In Patients With Recurrent Ovarian Cancer And Persistent Malignant Effusion.* (2023). <https://clinicaltrials.gov/study/NCT04919629>
41. Roumenina LT, Daugan MV, Petitprez F, Sautes-Fridman C, Fridman WH. Context-dependent roles of complement in cancer. *Nat Rev Cancer.* 2019;19(12):698–715. doi:10.1038/s41568-019-0210-0.
42. Ajona D, Ortiz-Espinosa S, Pio R, Lecanda F. Complement in metastasis: a comp in the camp. *Front Immunol.* 2019;10:669. doi:10.3389/fimmu.2019.00669.
43. Gunn L, Ding C, Liu M, Ma Y, Qi C, Cai Y, Hu X, Aggarwal D, Zhang H-G, Yan J, et al. Opposing roles for complement component C5a in tumor progression and the tumor microenvironment. *J Immunol.* 2012;189(6):2985–2994. doi:10.4049/jimmunol.1200846.
44. Kwan WH, van der Touw W, Paz-Artal E, Li MO, Heeger PS. Signaling through C5a receptor and C3a receptor diminishes function of murine natural regulatory T cells. *J Exp Med.* 2013;210(2):257–268. doi:10.1084/jem.20121525.
45. Gerard NP, Lu B, Liu P, Craig S, Fujiwara Y, Okinaga S, Gerard C. An anti-inflammatory function for the complement anaphylatoxin C5a-binding protein, C5L2. *J Biol Chem.* 2005;280(48):39677–39680. doi:10.1074/jbc.C500287200.
46. Vadrevu SK, Chintala NK, Sharma SK, Sharma P, Cleveland C, Riediger L, Manne S, Fairlie DP, Gorczyca W, Almanza O, et al. Complement c5a receptor facilitates cancer metastasis by altering T-cell responses in the metastatic niche. *Cancer Res.* 2014;74(13):3454–3465. doi:10.1158/0008-5472.CAN-14-0157.
47. Ricklin D, Lambris JD. Complement in immune and inflammatory disorders: therapeutic interventions. *J Immunol.* 2013;190(8):3839–3847. doi:10.4049/jimmunol.1203200.
48. Hirano F, Kaneko K, Tamura H, Dong H, Wang S, Ichikawa M, Rietz C, Flies DB, Lau JS, Zhu G, et al. Blockade of B7-H1 and PD-1 by monoclonal antibodies potentiates cancer therapeutic immunity. *Cancer Res.* 2005;65(3):1089–1096. doi:10.1158/0008-5472.1089.65.3.
49. Armstrong DK, Alvarez RD, Backes FJ, Bakkum-Gamez JN, Barroilhet L, Behbakht K, Berchuck A, Chen L-M, Chitiyo VC, Cristea M, et al. NCCN guidelines<sup>®</sup> insights: ovarian cancer, version 3.2022. *J Natl Compr Canc Netw.* 2022;20(9):972–980. doi:10.6004/jnccn.2022.0047.
50. Burger RA, Brady MF, Bookman MA, Fleming GF, Monk BJ, Huang H, Mannel RS, Homesley HD, Fowler J, Greer BE, et al. Incorporation of Bevacizumab in the primary treatment of ovarian cancer. *N Engl J Med.* 2011;365(26):2473–2483. doi:10.1056/NEJMoa1104390.
51. Kaufman B, Shapira-Frommer R, Schmutzler RK, Audeh MW, Friedlander M, Balmaña J, Mitchell G, Fried G, Stemmer SM, Hubert A, et al. Olaparib monotherapy in patients with advanced cancer and a germline BRCA1/2 mutation. *J Clin Oncol.* 2015;33(3):244–250. doi:10.1200/JCO.2014.56.2728.
52. Cancer Genome Atlas Research Network. Integrated genomic analyses of ovarian carcinoma. *Nature.* 2011;474(7353):609–615. doi:10.1038/nature10166.